CrossMark

ORIGINAL PAPER

Experimental study on hydrodynamic performances of naval propellers to adopt new additive manufacturing processes

Gabriele Staiano[1] · **Antonio Gloria**[2] · **Giovanni Ausanio**[3] · **Antonio Lanzotti**[1] · **Claudio Pensa**[1] · **Massimo Martorelli**[1]

Abstract In the past few years, a new generation of additive manufacturing (AM) techniques has rapidly become available due to the expiration of some AM patents which allowed significant cost reductions. This article explores some available techniques fostering products innovation in experimental laboratories for the development of naval propulsion, where high costs represent an important limitation for both basic research and industrial testing, by identifying significant knowledge and variables and by providing reliable and accurate data to support designers and researchers. The propeller INSEAN E779a case study was taken into account and fabricated by direct metal laser sintering in AlSi10Mg aluminium alloy and by fused deposition modeling in acrylonitrile–butadiene–styrene, and UltraT polymeric materials. The study of printing parameters, flexural tests, differential scanning calorimetry and thermogravimetric analysis, allowed to optimize the printing process conditions. A reverse engineering system, Faro-CAM2, and the iterative closest point algorithm of the geomagic control software were used to analyse deviations from the printed propeller and the CAD nominal model. The atomic force microscopy test allowed to assess the morphological features and surface roughness of printed propellers. Towing Tank tests were carried out and the hydrodynamic performance comparison was analysed in terms of torque and drag. The results of this study show differences between the benchmark and AM propellers, as a function of the advance coefficient J, the morphological characteristics and the materials. However this study also shows a substantial adequacy of AM propellers in most studies carried out in Towing Tank.

✉ Massimo Martorelli
massimo.martorelli@unina.it

Gabriele Staiano
gabriele.staiano@unina.it

Antonio Gloria
antonio.gloria@unina.it

Giovanni Ausanio
ausanio@na.infn.it

Antonio Lanzotti
antonio.lanzotti@unina.it

Claudio Pensa
claudio.pensa@unina.it

1 Department of Industrial Engineering, University of Naples Federico II, P.le V. Tecchio 80, 80125 Naples, Italy

2 Institute of Polymers, Composites and Biomaterials-National Research Council of Italy, V.le J.F. Kennedy 54, 80125 Naples, Italy

3 CNR-SPIN and Department of Physics E. Pancini, Naples, Italy

1 Introduction

The ASTM F42 and the ISO TC261 committees on additive manufacturing (AM) technologies define AM as a "process of joining materials to make objects from three-dimensional (3D) model data, usually layer upon layer, as opposed to subtractive manufacturing methodologies" [1]. Common to AM technologies is the use of a computer, a 3D modelling software (CAD), machine equipment and layering materials. Once a CAD model is produced, the model data, usually converted in STL format, are first decomposed into a series of 2D, finitely thick cross sections, which are then fed into an AM machine which lays downs or adds successive layers of liquid, powder, sheet material or others, in a layer-upon-layer fashion to fabricate a 3D object in metallic, plastic,

ceramic, composite, or biological materials. AM processes are used in different fields of applications and they have many advantages over traditional manufacturing processes such as a cost-effective and time-efficient way to produce low-volume, customized products with complicated geometries and advanced material properties and functionality, material waste is greatly reduced [2,3]. From the first patent registered on March 11th 1986 by Hull up to the present day, AM have evolved into different kinds of processes, including stereolithography (SLA), fused deposition modeling (FDM), laminated object manufacturing (LOM), selective laser sintering (SLS), selective laser melting (SLM), direct metal deposition (DMD), laser metal deposition (LMD), inkjet printing, and others. AM techniques, for several advantages which were previously mentioned, may be used for the construction of marine propellers, whose production process has remained virtually unchanged over the past decades, so that to respond to the needs of naval experimental laboratories (Towing Tank and cavitation tunnel) for which high costs are an important limitation for both basic research and industrial testing and for the creation of specialized design of customized propeller for fast boats (usually small) in order to overcome limitations due to high production costs, in relation to the commercial value of the product. This article explores a variety of techniques to show how a new technology (i.e. AM) can enable product innovation in this industrial sector by identifying significant knowledge and variables and by providing reliable and accurate data as references to support developers, designers and researchers. This study was carried out by analysing and comparing two AM techniques in order to assess their adequacy for the construction of marine propellers, for the towing tank open water propeller test, by combining their morphological data with the comparison of their hydrodynamic performance in respect to a benchmark propeller. In particular, a DMLS process was used to print an aluminium alloy propeller and a FDM process was used to print propellers in two different types of thermoplastic materials. The procedures used were specialized according to the intrinsic requirements of propellers and the chemical and physical characteristics of materials. The study on printing parameters and accurate physical-chemical and mechanical tests on the thermoplastic materials allowed to optimize process conditions.
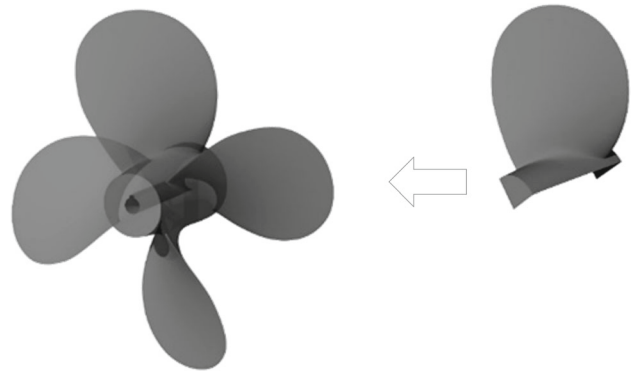
2 Materials and methods

2.1 Benchmarking propeller

The propeller INSEAN E779a case study, which is considered an adequate benchmark in literature, was considered. The E779a (Fig. 1) is a four blade right-handed propeller, Wageningen modified type, with a diameter of 227.27 mm,
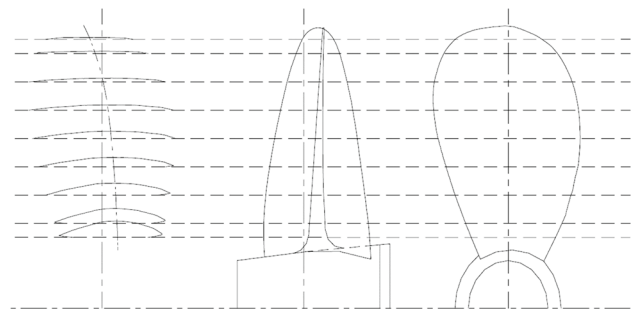
Fig. 1 The INSEAN E779a propeller

Fig. 2 E779a propeller CAD model

a forward rake angle of 4° 3", blade skew and rake are small, and the pitch ratio is almost constant along the radius (pitch/diameter = 1.1).

Performance characteristics in terms of dimensionless thrust K_T and torque K_Q coefficients, depending on the advance coefficients J were provided by INSEAN. According to the ITTC (International Towing Tank Conference) recommended procedures [4,5], the dimensionless K_T, K_Q and the J coefficient were defined as:

$$K_T = \frac{T}{\rho n^2 D^4}; \quad K_Q = \frac{Q}{\rho n^2 D^5} \quad \text{and} \quad J = \frac{V}{nD}$$

where T (N) and Q (N · m) were the propeller thrust and torque, n (rps) was the propeller rotational speed, D (m) the propeller diameter and ρ(kg/m^3) was the water density. Starting from the mathematical description of one blade (IGES), a new solid geometrical model was prepared in the Rhinoceros V5 CAD software, by Robert McNeel, and used in the present work (Fig. 2).

2.2 The AM process

Among the different AM technologies currently available, two techniques were considered in the present study: fusion deposition modeling (FDM) to print two propellers in two different thermoplastic materials and a DMLS, which allowed to manufacture the propeller in aluminium alloy. In order to optimize printing process conditions, studies about

the effects of the main printing process parameters, with respect to the produced parts, were carried out. Based on previous works [6–8] the analysis and the optimal setup of the printing process parameters for the FDM process were identified using a DoE approach. The DMLS is a typical AM process based on the layer by layer powder spreading and subsequent laser sintering [9]. Therefore, the DMLS enables the production of complex 3D shaped functional parts directly from metal powders. Based on the experience of experts and on literature reviews, a number of variables introduced by the DMLS process, such as laser scan speed, layer thickness, support structures and part orientation which contribute to the final geometric tolerances and surface roughness and which affect the final quality of the part, were taken into account. The main causes of variability in the DMLS process and the relative impact in the final characteristics of the printed part, are reported and grouped in relation to raw materials, model data preparation and setup of printing process in Tables 1, 2 and 3.

Table 1 Sources of variability in DMLS processes due to the properties of materials

Material property	Material property
Particle size distribution	Sinterability/meltability
	Packing efficiency
	Surface roughness
Particle shape	Packing efficiency
Apparent/tap density	Packing efficiency
Melting point	Indicator of energy requirements
Strength of green part	Facilitates part handling before thermal cycle (debinding, sintering, infiltration)
Specific heat, thermal conductivity	Heat transfer in powder bed
Void fraction	Residual porosity in printed parts
Flowability	Uniform spreading of powder layer

Table 2 Sources of variability in AM processes due to ambient conditions

Geometric/topological parameter	Affected characteristic
High temperature in room	Overload of the cooling system
	Inadequate cooling of the optical assemblies
	Formation of condensed water on cooled assemblies
Low temperature in room	Formation of condensed water on trim panels and housings
High ambient moisture content in room	Formation of condensed water on trim panels and housings
Inadequate supply of inert gas	Building process is interrupted

Open literature, which focuses on the fundamentals of the laser sintering process and the evaluation of materials produced by this method, and looks at mechanical properties and microstructure, have investigated the application of DMLS to the actual component quality. Some of these studies have quantified the surface roughness and the effect of process variables on the final part quality. Simchi et al. [10] have studied a simple iron-based DMLS part and reported surface roughness while Khaing et al. [11] have reported roughness for a nickel–bronze–copper DMLS part evaluating in addition the geometric tolerance of the test specimen. Senthilkumaran et al. [12] and Song and Koenig [13] have investigated the effect of various DMLS process parameters (laser scan speed, laser power, and hatching distance) on the surface roughness. Delgado et al. [14] have studied, in addition, the effect of the build direction on surface roughness and dimensional tolerance for stainless steel DMLS parts. Wong et al. [15] have examined heat transfer and pressure loss through additively manufactured heat exchangers. Calignano et al. [16] have investigated the effect of various DMLS process parameters by studying the DMLS of the AlSi10Mg powder through an experiment based on the Taguchi approach in order to assess the influence of processing parameters (hatching distance, scan speed and laser power) on surface roughness. It was found that low scan speeds resulted to improve the top surface finish by giving the melt pools more time to flatten before solidification. On the other side, a too low scan speed could increase the volume

Table 3 AM process variability due to geometrical and topological settings

Geometric/topological parameter	Affected characteristic
Part inclination (build angle)	Mechanical properties
	Part accuracy
	Process speed
Part positioning on the plate	Mechanical properties
	Part accuracy
	Shrinkage/distortion
Part orientation	Mechanical properties
	Part accuracy
	Shrinkage/distortion
Type and number of supports	Mechanical properties
	Process speed
	Wasted material amount
	Surface roughness
Z-height	Process speed
	Part accuracy
	Surface roughness
Layer thickness	Mechanical properties
	Part accuracy
	Process speed

of the liquid produced within the melt pool and the balling phenomenon could arise. In relation to laser power, higher values resulted in reducing the melt pool tendency to undergo balling by relieving surface tension variations. However, if laser power is too high, material vaporization can occur and recoil pressures can disrupt the melt pool surface. Read et al. [17] have investigated the influence of SLM process parameters on the porosity development in AlSi10Mg by means of the DOE approach, focusing on laser power, scan speed, scan spacing and island size. Experimenters have identified a low energy density region corresponding to a high porosity due to the lack of consolidation and a high energy density region (approximately over 60 J/mm^3) where other defects, such as keyhole formation (due to vaporization), had been observed within the material. This information allows to evaluate and optimize correct DMLS printing process conditions.

2.3 Analysis of materials

Concerning the materials used in this study, two types of thermoplastic polymers provided by Zortrax S.A., Poland, under the trade names of Z-ABS and Z-UltraT, were used to print propellers through the FDM process whereas a powder of aluminium alloy, AlSi10Mg, was used to print the propeller in metal alloy by means of the DMLS process. Differential scanning calorimetry (DSC) and thermogravimetric analysis (TGA) were carried out on polymeric materials. Specifically, the DSC analysis was performed on Z-ABS and UltraT at 10 °C/min, according to ASTM D3417 [18] and ASTM D3418 [19]. This test method determines the heat of fusion and the heat of crystallization of polymers by DSC. On the other hand, TGA is a method of thermal analysis in which changes in chemical and physical properties of materials are evaluated as a function of increasing temperature at a constant heating rate, or as a function of time at a constant temperature and/or constant mass loss. TGA may provide information about physical phenomena, such as second-order phase transitions, including absorption, adsorption, desorption, sublimation and vaporization. TGA relies on a high degree of precision in three measurements: mass change, temperature, temperature change. Three-point bending tests were performed on different kinds of printed "building blocks" made of Z-ABS and UltraT, according to ASTM D790 [20]. All tests were carried out using an Instron 5566 testing machine. The support span-to-depth ratio was 16–1.

2.4 The fabrication of AM propellers

The open-source RepRap Prusa Mendel Iteation 3 3D printer with a 0.35 mm nozzle diameter was used to fabricate the propellers with 1.75 mm filaments diameter in Z-ABS and Z-UltraT material. The 3D printer was assembled in two days at the Fraunhofer Joint Lab IDEAS-CREAMI (Interactive

Table 4 Optimized setup of the main printing process parameters considered to print both the propellers

Main printing setting	ABS	UltraT
Layer thickness (mm)	0.1	0.1
Flow rate (%)	105	105
x–y deposition speed (mm/min)	1800	1800
z deposition speed (mm/min)	1000	1000
Fill density (%)	100	100
Bed temperature (°C)	80	80
Printing temperature (°C)	250	250
Outline overlap (%)	15	15

Fig. 3 The propeller printed in thermoplastic materials through the FDM process

Design and Simulation—Center of Reverse Engineering and AM Innovation) of the University of Naples Federico II and it was calibrated with an accuracy of ±10 μm by using the magnetic base dial indicator, Mitutoyo 2046-08 (Mitutoyo, Japan). The firmware open-source software Marlin and the Simplify 3D slicing software were used to generate G-code files and command and control the 3D printer for the fabrication of the desired parts. For both materials the main setup of the printing process parameters were reported in Table 4.
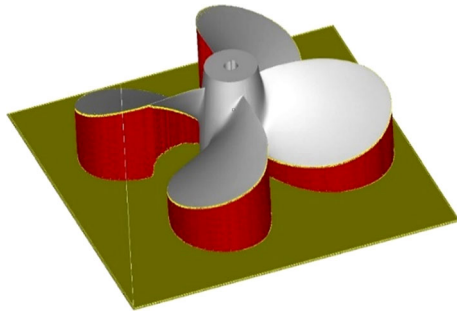
The printing process taken into account in this study required 59 h and about 180 m of filament to print both propellers in two thermoplastic materials (Fig. 3).

The EOS M280 DMLS Printer, courtesy of MBDA s.p.a. Italy, was used to print the propeller in the AlSi10Mg material. EOS has also provided metal printing powders together with production parameters (EOS Part Property Profiles, PPP), in order to have a producer certification, achieve minimum certified and repeatable mechanical performances and minimize every deviation from expected values.

Although PPP are conventionally locked, EOS provided, upon customer request, several unlocked profiles. The latter were given with standard values which should be equivalent, according to EOS, to the corresponding ones of the locked PPPs. Starting from these values, exposition parameters (Table 5) can be customized with respect to the actual needs, by using the Exposure Editor panel.

Table 5 Main DMLS exposure parameters

Exposure parameter	Value
Laser power	370 W
Scanning speed	1300 mm/s
Layer thickness	0.02 mm
Hatching distance	0.19 mm

Fig. 6 The cloud point of the propeller printed in ABS

Fig. 4 The preparation of the DMLS printing model in Magics software

Fig. 7 The cloud point of the propeller printed in UltraT

By using the MAGICS software by Materialise® and the RP-Tools by EOS, the STL model of the propeller was positioned and oriented on the build platform taking into account problems due to the flows of the inert gas within the print volume and impacts due to the passage of the coater (Fig. 4).

As a consequence, it was possible to create support structures, bearing in mind the countless critical issues in executing this step, such as removability, surface quality alteration and heat drain from the part.

The building platform was preheated at 200 °C and the printing process required 28 h and 30 min. In this process a post-processing phase was needed, with a stress relieving cycle of 2 h at 300 °C and supports removal (Fig. 5).

2.5 Shape quality inspection, morphological and roughness evaluation of printed propellers

A high resolution non-contact laser scanner, articulated arm coordinate measuring machines (AACMM) Faro CAM2 Sca-

nArm HD was used to acquired and generate the cloud points of ABS (Fig. 6), UltraT (Fig. 7) and AlSi10Mg (Fig. 8) printed propeller. The accuracy of this non-contact Reverse Engineering system is of ±25 μm. All scan data were post-processed in the Geomagic Control software by 3D Systems using an iterative closest point algorithm [21] to align and minimize the distance between clouds point and the nominal CAD model.
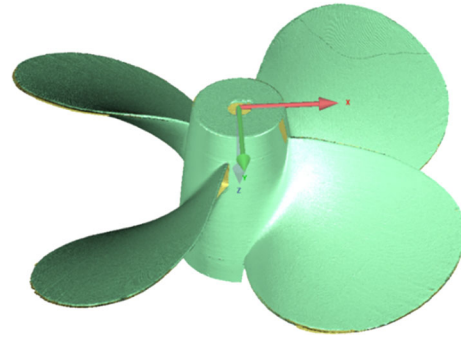
As shown in Table 6 the three acquired clouds were made of a number of points which can be compared with one another.

The atomic force microscopy (AFM) analysis was performed on specimens obtained from the blade of two polymer-based propellers.
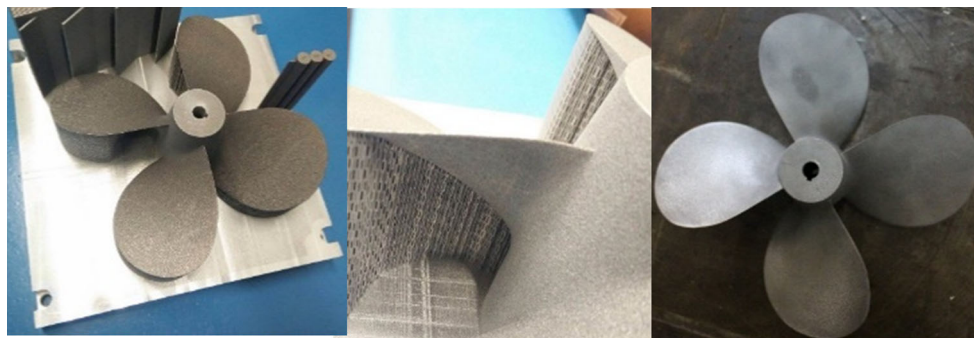
Fig. 5 The DMLS printed propeller before and after supports removal
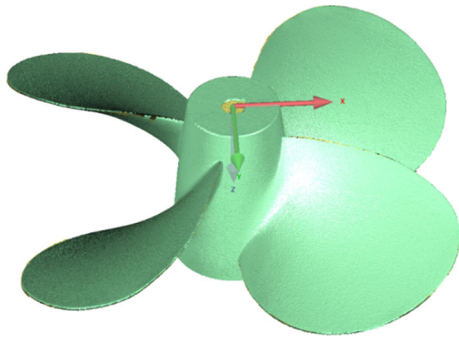
Fig. 8 The cloud point of the propeller printed in AlSi10Mg

Table 6 Number of points relative each acquired propeller

Cloud point	Number of points
AlSi10Mg	2,469,684
UltraT	2,336,531
ABS	2,392,902

The imaging was performed in tapping mode.

Three different AFM imaging modes can be usually considered: a) contact mode, where the deflection of the cantilever is kept constant; b) non-contact mode, where the tip is oscillated at the resonance frequency and the amplitude of the oscillation is kept constant; c) tapping mode, which is somewhere between the contact and non-contact mode.

Specifically, the amplitude is set at about 100 % of "Free" amplitude; and at about 50–60 % of "Free" amplitude for non-contact mode and tapping mode, respectively.

However, the tapping mode provides higher resolution with minimum sample damage.

2.6 Towing tank tests

Following the current procedures recommended by the International Towing Tank Conference (ITTC), towing tank open water propeller tests were performed with the sampling frequency of 1 kHz on the three printed propellers. The comparison of the hydrodynamic performance between them and the benchmark, in terms of trust and torque, was carried out. Experimental tests were performed in the towing tank of the Naval Section of the Department of Industrial Engineering of the University of Naples Federico II (Fig. 9). The towing tank is 136.5 m long, 9 m large and 4.5 m deep. It allows a maximum speed of 10 m/s with an acceleration of 1 m/s^2 and a deceleration of 3 m/s^2.

The towing tests were performed by using propeller dynamometers called H29 (Fig. 9). As suggested by the ITTC procedures [4], the Reynolds number (Re) of open water propeller tests was calculated in relation to cord measured at 0.7 of the radius (Re$_{0.7R}$), which is usually considered represen-

Fig. 9 The Towing Tank test using H29 propeller dynamometers
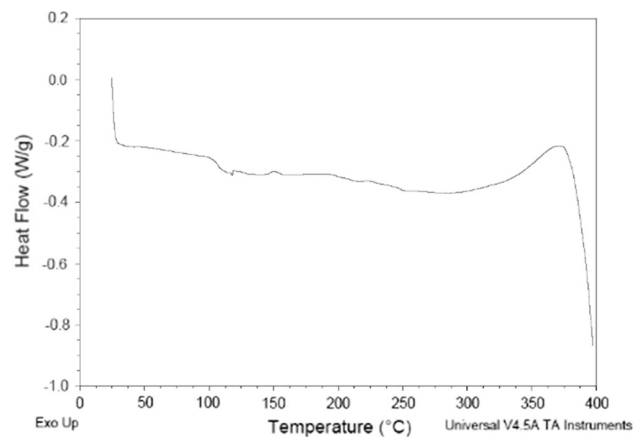
Fig. 10 DSC analysis: typical curve of heat flow versus temperature for Z-ABS
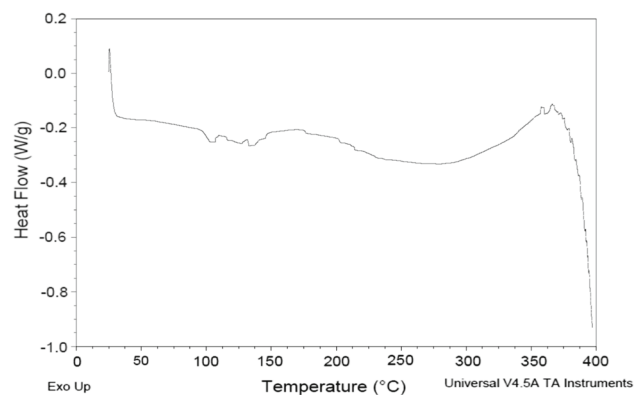
Fig. 11 Typical curve of heat flow versus temperature for Z-UltraT

tative of the performance of the entire blade. The procedure used to obtain the dimensionless thrust K_T and torque K_Q coefficients, as a function of the advance coefficient J, which was previously defined, involves to vary the tank dynamometer speed V and keep the propeller revolutions n constant.
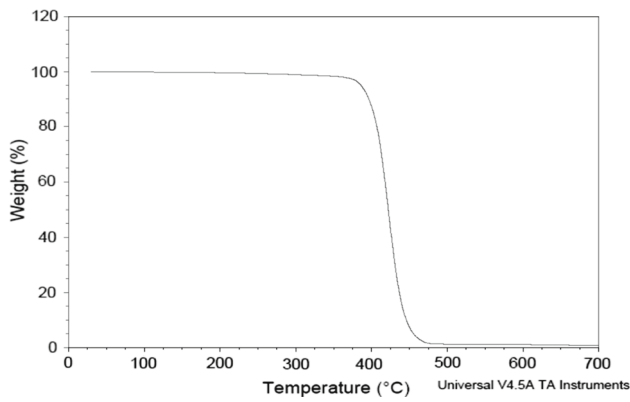
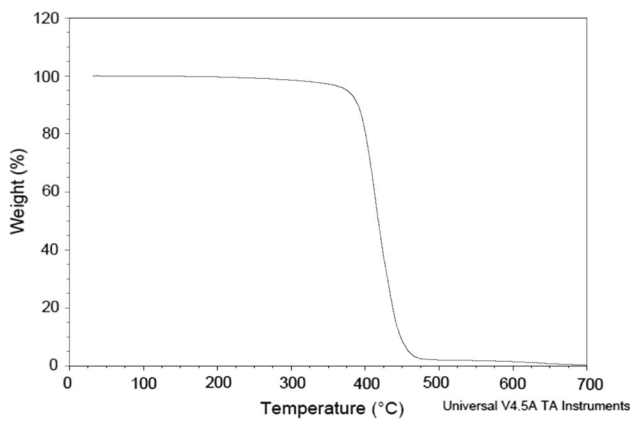Fig. 12 TGA: typical weight versus temperature curve for Z-ABS

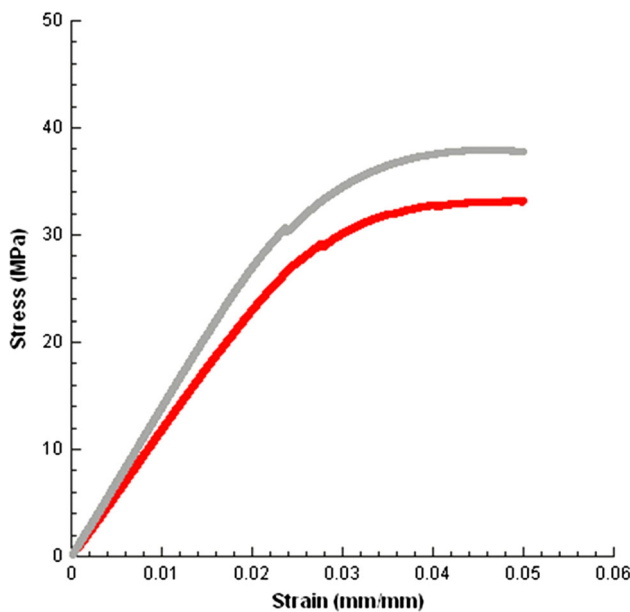Fig. 13 TGA: typical weight versus temperature curve for Z-UltraT

Table 7 Results from three-point bending: modulus (E) and maximum stress (σ_{max}) reported as mean value $\pm$ standard deviation

Sample	E (MPa)	$\sigma_{max} = \sigma_{fc}$ (MPa)
Z-ABS	1202.9 ± 24.0	33.2 ± 0.1
Z-ULTRA T	1422.4 ± 19.7	37.9 ± 0.4

3 Results

3.1 Calorimetric analysis of thermoplastic materials

Results from the DSC analysis performed on Z-ABS and Z-UltraT were reported in terms of heat flow-temperature curves (Figs. 10, 11).

Results from TGA performed on Z-ABS and Z-UltraT were reported in terms of weight-temperature curves (Figs. 12, 13).

3.2 Flexural tests

Stress–strain curves obtained from three-point bending tests on two different kinds of printed "building blocks" made of Z-ABS and Z-UltraT evidenced similar stress–strain curves (Fig. 14).
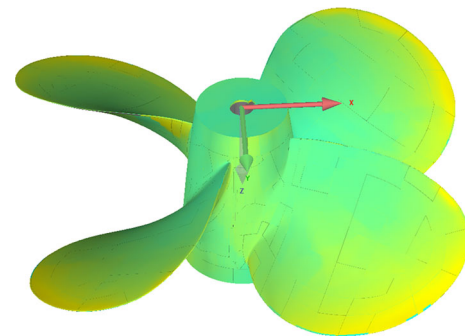

Fig. 15 Graphical evaluation of distances between the point cloud of the propeller in AlSi10Mg and the 3D CAD nominal model

Fig. 14 Typical stress–strain curves obtained from three-point bending tests on two different kinds of printed "building blocks" made of Z-ABS (*red line*) and Z-UltraT (*grey line*) (colour figure online)
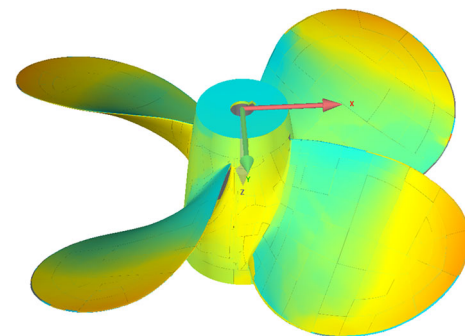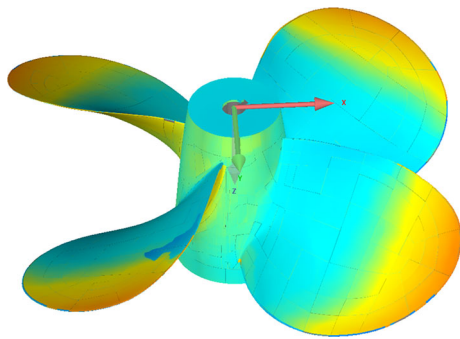

Fig. 16 Graphical evaluation of distances between the point cloud of the propeller in UltraT and the 3D CAD nominal model

Fig. 17 Graphical evaluation of distances between the point cloud of the propeller in ABS and the 3D CAD nominal model

Table 8 Number of points for each acquired propeller

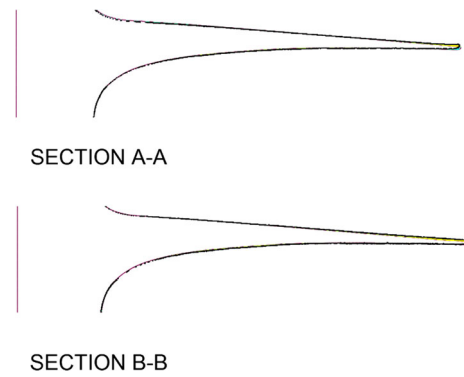| Cloud point	Average (mm)	Standard deviation (mm)
AlSi10Mg	0.12/−0.08	0.14
UltraT	0.47/−0.29	0.56
ABS	0.49/−0.56	0.69
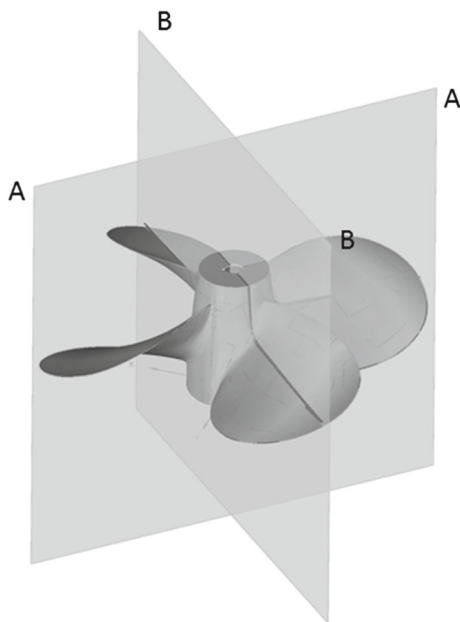
Fig. 18 Planes used to section the point cloud of the propeller aligned with the CAD model in 2D analysis

Fig. 19 Single blade 2D comparison between sections of the point cloud of the propeller in AlSi10Mg and the 3D nominal CAD model

Fig. 20 Single blade 2D comparison between sections of the point cloud of the propeller in UltraT and the 3D nominal CAD model

Fig. 21 Single blade 2D comparison between sections of the point cloud of the propeller in ABS and the 3D nominal CAD model
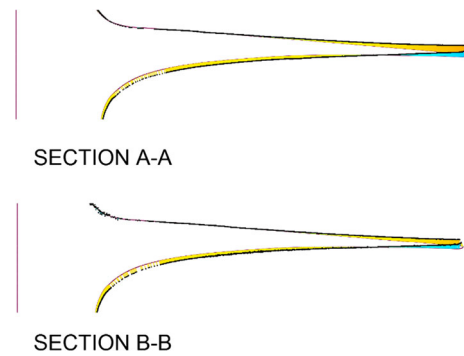
The bending modulus (i.e., the slope of the linear region of the curve) and the maximum stress were evaluated and reported as mean value ± standard deviation (Table 7).
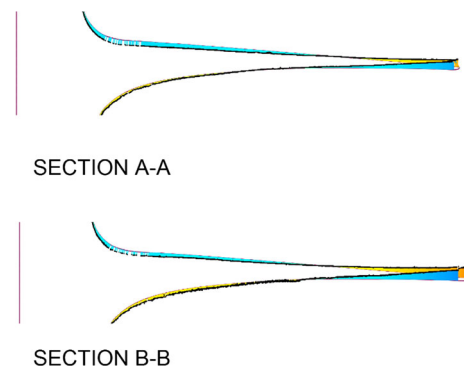
3.3 Reverse engineering analysis

Based on a strict protocol [22] in order to get highly repeatable measurements, the use of well-defined features as references (see also fixtures) was considered during the align-

ment phase of the cloud point with the nominal CAD model. Standard deviation was considered as a good measure for accuracy. All distances between each point cloud and the 3D CAD nominal model were analysed. Figures 15, 16 and 17 show the chromatic map of distances between point clouds and the nominal CAD model related to a value of standard deviation reported in Table 8.

The 2D deviation analysis was carried out by sectioning the acquired cloud points, of each propeller, aligned with the CAD model, with the plans as shown in Fig. 18.

Table 9 2D analysis between section of points cloud aligned to CAD model for each propeller

Cloud point	Section	Standard deviation (mm)
AlSi10Mg	A–A	0.15
	B–B	0.14
UltraT	A–A	0.50
	B–B	0.57
ABS	A–A	0.66
	B–B	0.79

Figures 19, 20 and 21, show the comparison of the 2D section, between point clouds and the nominal CAD model, relating to a value of standard deviation reported in Table 9.

### 3.4 Atomic force microscopy (AFM) analysis

The AFM analysis allowed to assess morphological features, surface roughness and topography of the two samples related to the employed manufacturing technology (Figs. 22, 23). In

particular, a root mean square roughness (Rms) of 0.2–1.4 nm was evaluated.

3.5 Hydrodynamic performance analysis and comparison between printed propellers and benchmark

In Fig. 24, the results of hydrodynamic characteristics, in terms of thrust generated by the propellers, through the K_T dimensionless coefficient, were plotted and compared while, in Fig. 25, the results of hydrodynamic characteristics, in terms of torque absorbed by the propellers, through the K_Q dimensionless coefficient, were plotted and compared. Moreover, having carried out the measures at 1 kHz sampling frequency, the Fast Fourier transforms (FFT) method was used to analyze spectral characteristics of the torque of printed propellers for three values of the advance coefficient J (Figs. 26, 27, 28). Spectral amplitude was obtained by applying an averaging technique with a hamming window. The amplitude field of interest required the application of a band filter below 10 Hz and above 50 Hz.
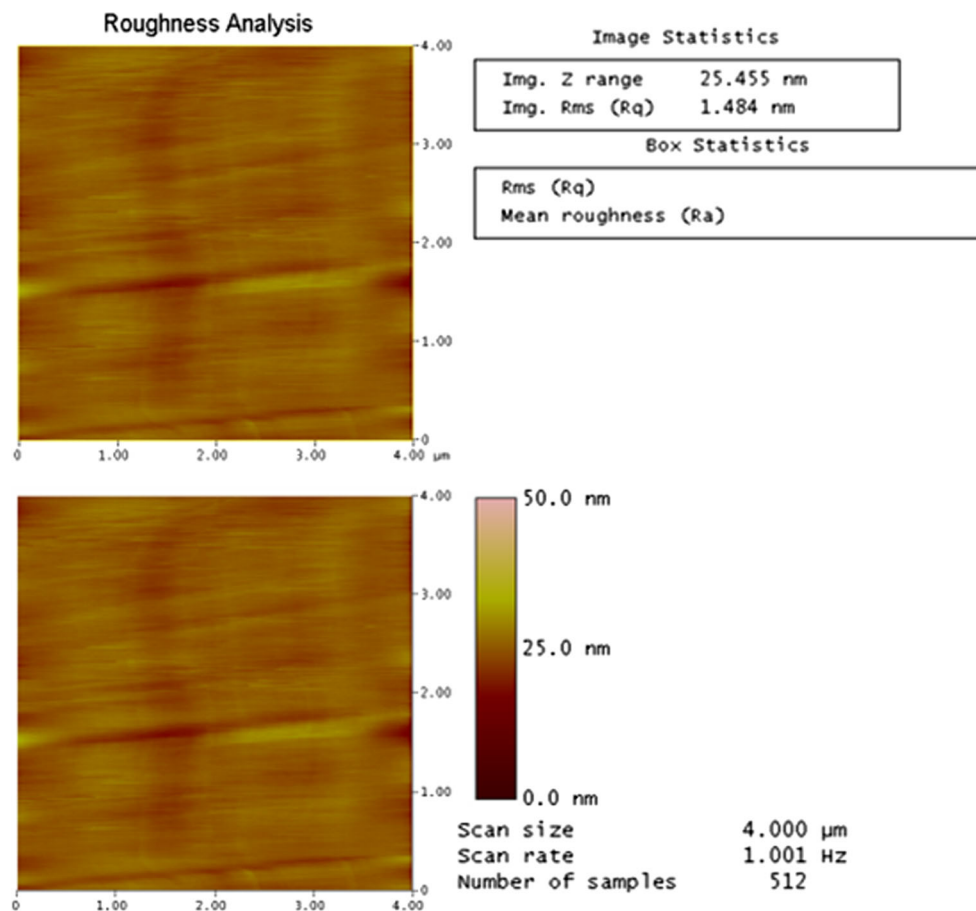
Fig. 22 Results obtained from AFM performed on Z-ABS: roughness analysis
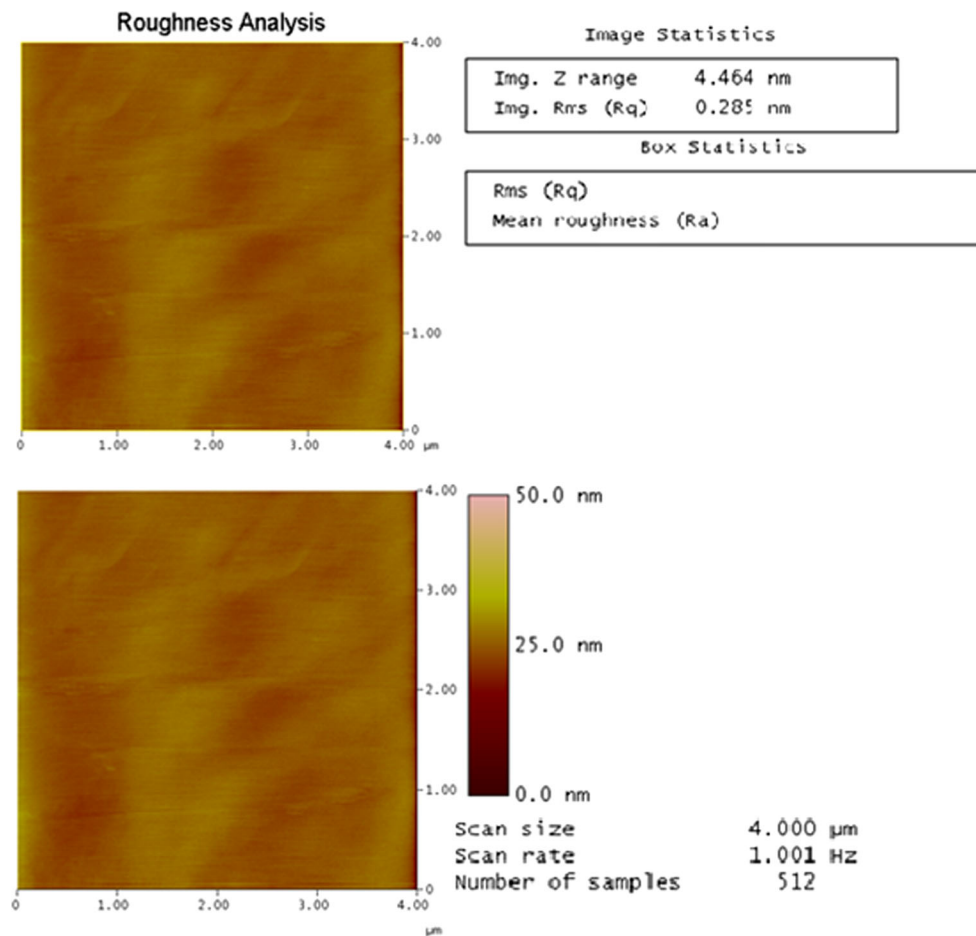
Fig. 23 Results obtained from AFM performed on Z-UltraT: roughness analysis

4 Discussion

Glass transition temperatures of about 125 and 144 °C were evaluated for Z-ABS and Z-UltraT, respectively. Results from TGA allowed to assess the thermal stability of materials.

Accordingly, in a specific temperature range, if a species is thermally stable, no mass change is observed. Negligible mass loss corresponds to little or no slope in the TGA trace. TGA provides the upper use temperature of a material and beyond this temperature the material begins to degrade, thus providing interesting information in terms of process parameters.

An initial linear region of the stress–strain curve was evident. Then, a decrease of the slope was observed. According to ASTM D790 [18] as all specimens neither yield nor break before the 5 % limit, σ_{max} was equal to σ_{fc} (flexural stress at 5 % strain limit).

As reported in Table 7, Z-UltraT provided the highest values for both the bending modulus and the maximum stress than the ones provided by Z-ABS.

As shown, the three-dimensional comparison between point clouds acquired by the RE technique and the CAD model, showed the greatest accuracy given by the DMLS process evidenced by the lower standard deviation of the propeller printed in AlSi10Mg, compared to propellers printed in thermoplastic materials using the FDM process. In particular, between the last two, the propeller printed in ABS presents greater deviations from the nominal model than the propeller printed in UltraT.

This variation could be mainly attributed to problems due to the higher shrinkage of ABS compared to UltraT.

The comparison between the two-dimensional sections A–A and B–B, of point clouds, aligned with the CAD model, showed a substantial polar symmetry in the propeller printed in AlSi10Mg with the DMLS process which is evidenced by the comparable standard deviations between the two sections.

The propellers printed in thermoplastic materials, using the FDM process, showed a polar asymmetry due to the shrinkage associated to this AM process and dependent on the material used.
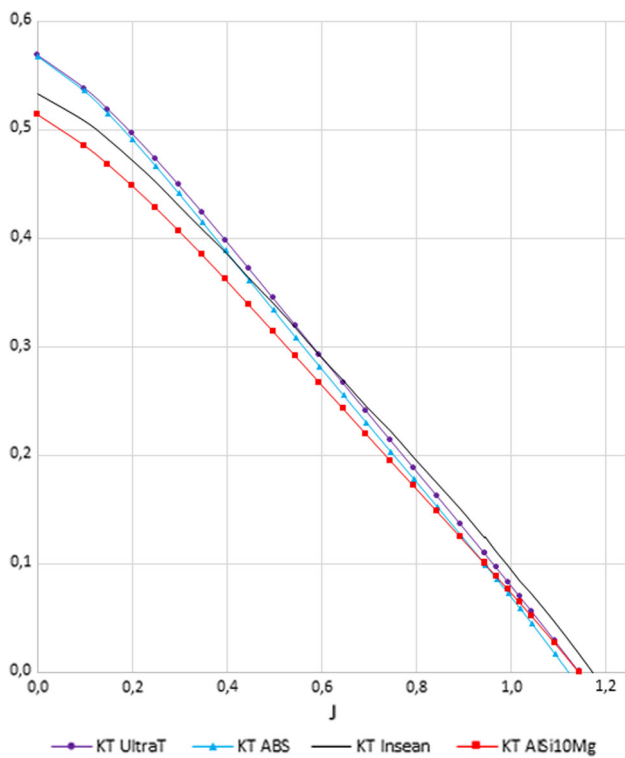
Fig. 24 Comparison of the KT coefficient of the three printed propellers to the benchmark
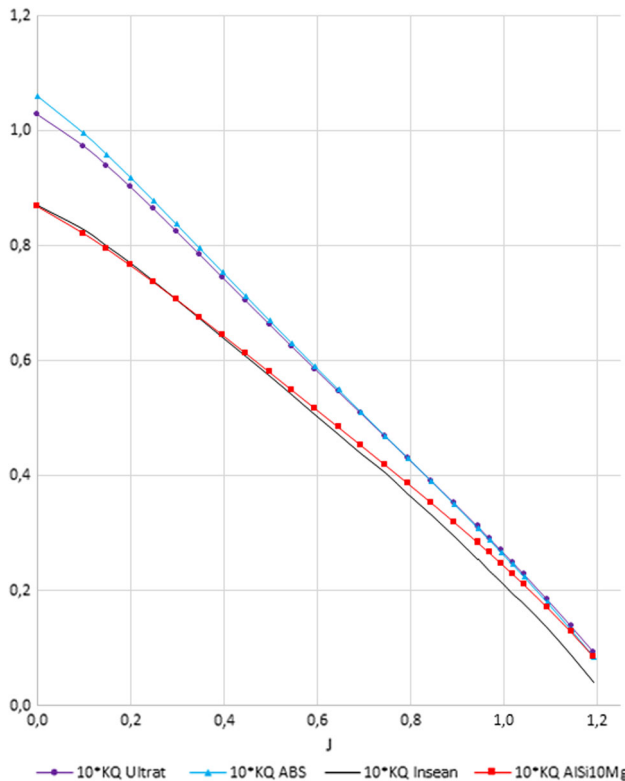
Fig. 25 Comparison of the K_Q coefficient of the three printed propellers to the benchmark
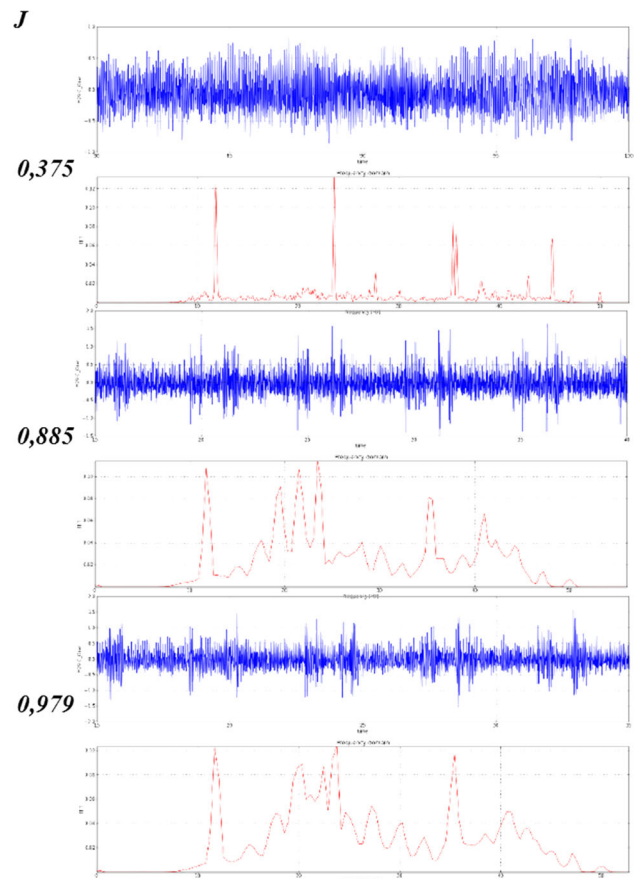
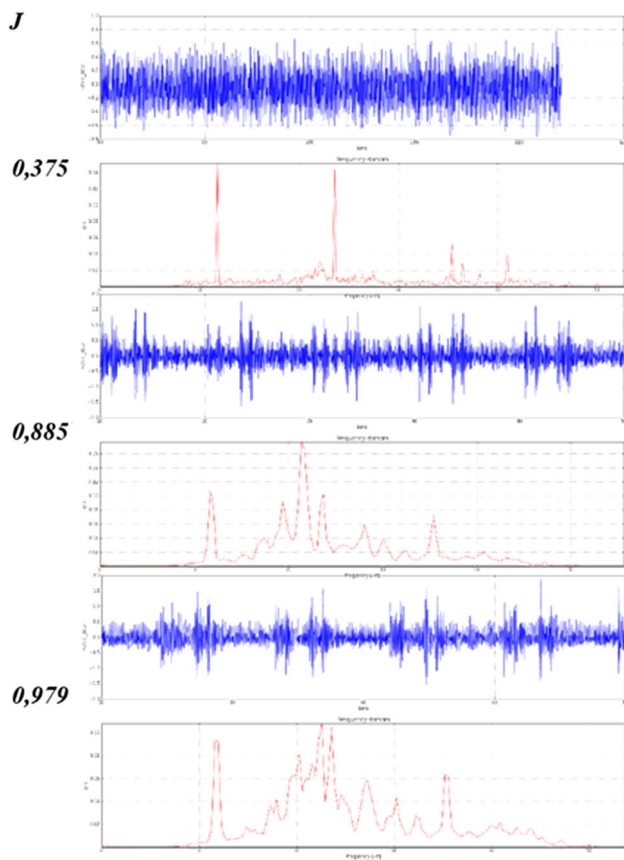**Fig. 26** Time-frequency analysis of experimental data of the AlSi10Mg propeller

In particular, the propeller printed in ABS showed major asymmetries, then the propeller printed in UltraT.

This was also evidenced by the higher difference in the standard deviation value, which was obtained by the bidimensional comparison between the points cloud and the nominal CAD model. The comparison between the dimensionless thrust coefficients, K_T, shows a substantial coincidence of the characteristic curves.

The curves of K_T, related to propellers printed in UltraT and ABS, coincided with each other and both had higher values than the benchmark curve at low J. The curve of K_T related to the propeller printed in AlSi10Mg presents, for each J, lower values compared to the benchmark of an almost constant amount.

On the contrary, regarding the characteristic curves related to torque absorption, for propellers in ABS and UltraT, the curves of K_Q coincided with each other and, compared to the benchmark, have higher values in relation to low J or when the propeller work in load conditions.

For the propeller printed in AlSi10Mg, the characteristic curve of K_Q generally coincided with the benchmark with slightly higher values to high J or when the propeller works discharges.
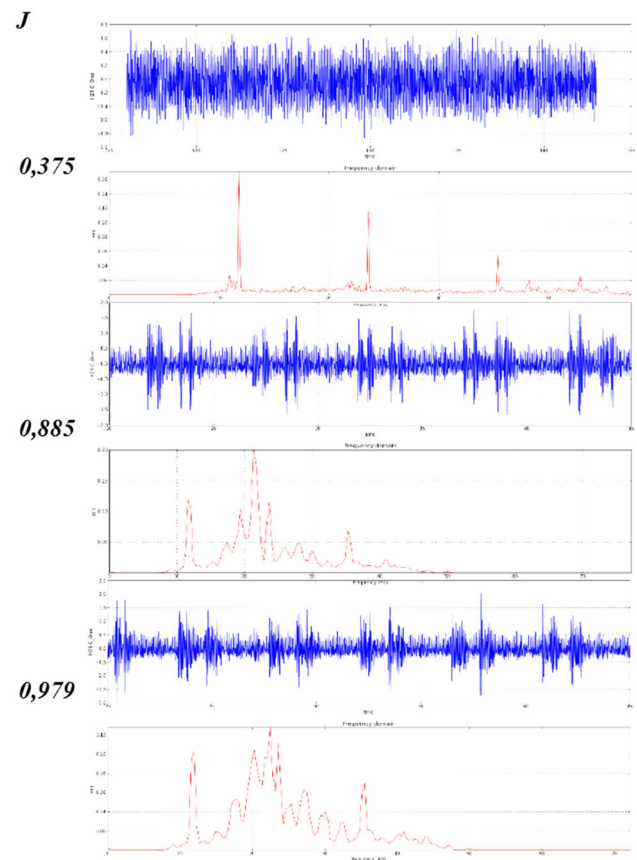
Fig. 27 Time-frequency analysis of experimental data of the UltraT propeller

Fig. 28 Time-frequency analysis of experimental data of the ABS propeller

The differences in performance between printed propellers and the benchmark can be due to:

– geometry variations, with respect to the original propeller, due to the RE process which led to the geometry to be used for the generation of the initial CAD model;
– geometrical variations, quantified in the shape control phase by RE techniques, due to the printing process;
– the polar asymmetries due to shrinkage related to materials and printing processes considered;
– the mechanical characteristics detected by the flexural test;
– the morphological characteristics and the surface roughness measured by the AFM analysis.

Concerning the propeller manufactured in thermoplastic materials, the main differences from the benchmark were found in increases of the absorbed torque at low values of J or when the propellers work under load.

In this condition, the variations can be mainly attributed to the deformation of the material used which involves a change in the effective pitch of the blade section [23].

For the propeller made of aluminum alloy it was found a high value related to the surface roughness in comparison to the benchmark propeller.

This problem could be the main cause of the constant low values of AlSi10Mg in K_T in comparison to the benchmark [24].

As shown in Figs. 26, 27 and 28, when the propeller is charged at low J there are four increments of amplitude coinciding with the modals related to blade passages in all printed propellers.

For the values of J, in which propellers operate in more discharged conditions, an increment of amplitude of the second modal was detected in propellers in thermoplastic material.

This phenomenon, which could be attributed to residual polar asymmetries due to shrinkage associated with AM processes, was the input to perform the two-dimensional analysis on propeller sections which confirmed this assumption.

Furthermore, this effect was not noticeable at low values of J due to other effects, such as bending of the blades, which were predominant.

The steps followed in this research and their effect on the results are summarized in Table 10.

Table 10 Steps followed in the research and their effect on the results

Step	Analysis and test	Results
Study of printing parameters	DoE	Optimization of process conditions
Physical–chemical analysis	DSC analysis TGA analysis	
Mechanical analysis	Flexural tests	Evaluation of mechanical performance
Morphological analysis	AFM test RE analysis	Evaluation of morphological performance and surface roughness
Hydrodynamic analysis	Towing Tank tests time–frequency analysis RE analysis	Evaluation on hydrodynamic performance of effects due to residual polar asymmetries

5 Conclusion

The main purpose of this research work regarded the analysis and the comparison of the hydrodynamic performance of marine propellers manufactured by using two AM techniques.

In particular a DMLS technique was used to print an aluminium alloy propeller and a FDM technique was used to print two propellers in different types of thermoplastic materials.

The approach followed in the paper uses different engineering processes to obtain the results summarised in the following considerations.

The study of printing parameters and accurate physical-chemical and mechanical tests on considered thermoplastic materials, allowed to optimize process conditions.

The mechanical analysis and the AFM test made it possible to evaluate mechanical and morphological performances.

The evaluation of printed propellers was carried out by combining their morphological and mechanical data with the comparison of their performance in relation to the benchmark.

In addition to that, having carried out measures at 1 kHz sampling frequency, effects of residual polar asymmetries due to shrinkage associated to the AM process on the hydrodynamic performance of propellers were evaluated.

The final analysis showed the substantial adequacy of AM propellers in most studies carried out in Towing Tank.

This is due both to reduced deviations from the nominal model, and to the verified constancy of performance offered by each prototype.

Future work on this research will improve the study of the effect of roughness on the hydrodynamic performance of printed propellers and evaluate the performance of propellers printed through the FDM process, using a polymeric composite reinforced with nanoparticles, in order to increase mechanical characteristics and get their hydrodynamic performance as close as possible to metal propellers manufactured with traditional processes.

References

1. ASTM F2792–10.: Standard terminology for additive manufacturing. In: ASTM international committee F42 on additive manufacturing. ASTM, West Conshohocken (2009)
2. Fantini, M., De Crescenzio, F., Ciocca, L.: Design and rapid manufacturing of anatomical prosthesis for facial rehabilitation. Int. J. Interact. Des. Manuf. (IJIDeM) **7**(1), 51–62 (2013)
3. Laverne, F., Segonds, F., D'Antonio, G., Le Coq, M.: Enriching design with X through tailored additive manufacturing knowledge: a methodological proposal. Int. J. Inter. Des. Manuf. (IJIDeM), 1–10 (2016)
4. ITTC.: Testing and extrapolation methods: propulsion, performance propulsion test. In: Tech. Rep. 7.5-02-03-01.1. International Towing Tank Conference (2002)
5. ITTC.: Testing and extrapolation methods: propulsion, propulsor open water test. In: Tech. Rep. 7.5-02-03-02.1. International Towing Tank Conference (2002)
6. Lanzotti, A., Del, Giudice, D., Lepore, A., Staiano, G., Martorelli, M., : On the geometric accuracy of RepRap open-source three-dimensional printer. J. Mech. Des. Trans. ASME **137**(1), 101703-1–101703-8 (2015)
7. Lanzotti, A., Grasso, M., Staiano, G., Martorelli, M., The impact of process parameters on mechanical properties of parts fabricated in PLA with an open-source 3-D printer. Rapid Prototy. J. **21**, 604–607 (2015)
8. Lanzotti, A., Martorelli, M., Staiano, G.: Understanding process parameter effects of reprap open-source three-dimensional printers through a design of experiments approach. J. Manuf. Sci. Eng. **137**(1), 011017-1–011017-7 (2015)
9. Khaing, M.W., Fuh, J., Lu, L.: Direct metal laser sintering for rapid tooling: processing and characterization of EOS parts. J. Mate. Process. Technol **113**, 269–272 (2001)
10. Simchi, A., Petzoldt, F., Pohl, H.: On the development of direct metal laser sintering for rapid tooling. J. Mater. Process. Technol **141**, 319–328 (2003)
11. Khaing, M.W., Fuh, J., Lu, L.: Direct metal laser sintering. J. Mater. **113**, 269–272 (2001)
12. Senthilkumaran, K., Pandey, P.M., Rao, P.V.M.: Influence of building strategies on the accuracy of parts in selective laser sintering. Mater. Des. **30**(8), 2946–2954 (2009)
13. Song, Y.A., Koenig, W.: Experimental study of the basic process mechanism for direct selective laser sintering of low-melting metallic powder. CIRP Ann. Manuf. Technol. **46**(1), 127–130 (1997)

14. Delgado, J., Ciurana, J., Rodrıguez, C.A.: Influence of process parameters on part quality and mechanical properties for DMLS and SLM with ron-based materials. Int. J. Adv. Manuf. Technol. **60**(5–8), 601–610 (2012)

15. Wong, M., Owen, I., Sutcliffe, C.J., Puri, A.: Convective heat transfer and pressure losses across novel heat sinks fabricated by selective laser melting. Int. J. Heat Mass transfer **52**(1–2), 281–288 (2009)

16. Calignano, F., Manfredi, D., Ambrosio, E.P., Iuliano, L., Fino, P.: Influence of process parameters on surface roughness of aluminum parts produced by DMLS. Int. J. Adv. Manuf. Technol. **67**(9–12), 2743–2751 (2013)

17. Read, N., Wang, W., Essa, K., Attallah, M.: Selective laser melting of AlSi10Mg: process optimisation and mechanical properties development. Mater. Des. **65**, 417–424 (2015)

18. ASTM-D3417.: Standard test method for enthalpies of fusion and crystallization of polymers by differential scanning calorimetry (DSC). ASTM International, West Conshohocken (1999)

19. ASTM-D3418.: Standard test method for transition temperatures and enthalpies of fusion and crystallization of polymers by differential scanning calorimetry. ASTM International, West Conshohocken (2015)

20. ASTM-D790.: Standard test methods for flexural properties of unreinforced and reinforced plastics and electrical insulating materials. ASTM International, West Conshohocken (2002)

21. Besl, P.J., McKay, N.D.: A method for registration of 3-D shapes. IEEE Trans. Pattern Anal. Mach. intell. **14**(2), 239–256 (1992)

22. Gerbino, S., Del Giudice, D., Staiano, G., Lanzotti, A., Martorelli, M.: On the influence of scanning factors on the laser scanner-based 3D inspection process. J. Adv. Manuf. Technol. **84**, 1787–1799 (2015)

23. Liu, P., Bose, N., Frost, R., Macfarlane, G., Lilienthal, T., Penesis, I.: Model testing and performance comparison of plastic and metal tridal turbine rotors. Appl. Ocean Res. **53**, 116–124 (2015)

24. Breteau, T., Damay, T., Duc, E., Hascoët, J.Y.: Design for manufacturing with tool paths adapted to marine propeller. Int. J. Inter. Des. Manuf. (IJIDeM) **5**, 271–275 (2011)